Weak ferromagnetism of Cu_{x}Fe_{1+y}As and its evolution with Co doping

Bin Qian, Jin Hu, Jinyu Liu, Zhida Han, Ping Zhang, Lei Guo, Xuefan Jiang, T. Zou, M. Zhu, C. R. Dela Cruz, X. Ke, and Z. Q. Mao

Phys. Rev. B **91**, 014504 — Published 12 January 2015

DOI: 10.1103/PhysRevB.91.014504

Weak ferromagnetism of $Cu_xFe_{1+y}As$ and its evolution with Co doping

Bin Qian[1,2*], Jin Hu[2], Jinyu Liu[2], Zhida Han[1], Ping Zhang[1], Lei Guo[1], Xuefan Jiang[1],T. Zou[3], M. Zhu[3], C. R. Dela Cruz[4], X. Ke[3] and Z.Q. Mao [2*]

1. *Advanced Functional Materials Lab and Department of Physics, Changshu Institute of Technology, Changshu 215500, China*
2. *Department of Physics and Engineering Physics, Tulane University, New Orleans, Louisiana 70118, USA*
3. *Department of Physics and Astronomy, Michigan State University, East Lansing, Michigan 48825, USA*
4. *Quantum Condensed Matter Division, Oak Ridge National Laboratory, Oak Ridge, Tennessee 37831, USA*

Abstract

We have investigated electronic and magnetic properties of iron pnictide $Cu_xFe_{1+y}As$, which is isostructural to iron pnictide superconductors LiFeAs and NaFeAs, using polycrystalline and single crystal samples. We found that $Cu_xFe_{1+y}As$ is characterized by strong electron correlations and shows weak ferromagnetic behavior with the Curie temperature $T_c \sim 42$ K, in contrast with the superconductivity in LiFeAs and NaFeAs. Its electronic transport properties exhibit quasi-two-dimensional characteristics: while the in-plane resistivity follows quadratic temperature dependence for $T < 10$K, the c-axis resistivity shows nonmetal-to-metal crossover near 20 K. In addition, we have studied Co doping effect on $Cu_xFe_{1+y}As$ and found that Co doping enhances the ferromagnetism with T_c increasing up to 83 K for $Cu_xFe_{0.5}Co_{0.5}As$. From these results, we discussed the origin of the ferromagnetism of $Cu_xFe_{1+y}As$ and its relevance with the magnetism of iron pnictide superconductor parent compounds

I. INTRODUCTION

The fact that the unconventional superconductivity in iron pnictides and chalcogenides is interplayed with magnetism motivated extensive research on the origin of antiferromagnetism of iron pnictide and chalcogenide superconductor parent compounds[1-10]. Iron pnictides parent compounds, such as LaOFeAs and $BaFe_2As_2$, exhibit "single-stripe" antiferromagnetic (AFM) order with the in-plane component of AFM wave vector along the Fermi surface (FS) nesting direction (*i.e.* ΓM direction) [11-12] . Such an AFM order was considered to be driven by FS, i.e., spin-density wave (SDW) induced by FS nesting [13-17]. However, for iron chalcogenide parent compound $Fe_{1+y}Te$, its AFM order [18-19] is distinct from those of iron pnictides though it shares similar FS with iron pnictides [20-22]: its AFM state is characterized by "double-stripe" order with the in-plane component of AFM wave vector along a direction 45° deviated from the FS nesting direction (*i.e.* Γ-X direction) [18-19]. With this result, the model of antiferromagnetism driven by the FS nesting appears to run into difficulties. Apart from the FS-driven magnetism, several models based on local moment superexchange interactions have been proposed [2-5, 9-10] and coupling between local moments and itinerant electrons have also been considered [1-2, 5-7].

Recently, a unified microscopic model, which can explain the antiferromagnetism of both iron pnictides and $Fe_{1+y}Te$, was proposed by Yin *et al*. [7]. The central idea of this model is that the AFM superexchange interaction between local moments competes with the ferromagnetic (FM) interaction mediated by the Hund's coupling between local moments and itinerant electrons. The key tuning parameter for these two competing magnetic interactions is the anion height (Z_{anion}) from the iron plane. With the increase of Z_{anion}, the magnetic ground state is predicted to evolve from a "single-stripe" AFM order, then to a "double-stripe" AFM order and finally to a FM order. Such a dependence of magnetic ground state on Z_{anion} was also demonstrated by the first-principles calculations [8]. The difference of Z_{anion} between iron pnictides (Z_{As} ~ 1.31-1.51 Å [11-12, 23]) and $Fe_{1+y}Te$ (Z_{Te} ~ 1.77 Å [18]) is quite consistent with the theoretical prediction that the switch from the "single-stripe" to "double-stripe" AFM order occurs as Z_{anion} is increased above 1.71 Å [8]. Our previous observation of itinerant ferromagnetism in CuFeSb provides further support for this unified model. CuFeSb shares a similar layered, tetragonal structure with LiFeAs and its

anion height from the iron plane Z_{Sb} is 1.84 Å [24]. The presence of ferromagnetism in this compound agrees well with the theoretically-predicted trend toward a FM state for a large anion height. These theoretical and experimental results point to a critical region of research, namely the borderline between the AFM and FM phases. This critical region may host strong quantum fluctuations, the proper understanding of which would greatly advance our understanding of the roles of electronic correlations in iron-based superconductors. $Cu_xFe_{1+y}As$ studied in this article is a promising candidate material for the study of physics of such a critical region. This material was first synthesized by Lv *et al.* [25] in polycrystalline form and recently reproduced by Thakur *et al*. [26]. Its structure also belongs to the Cu_2Sb type and is thus isostructural to CuFeSb and LiFeAs. The magnetic properties of this material reported by Lv *et al.* [25] and Thakur *et al.* [26] are not fully consistent. Lv *et al*. [25] reported that CuFeAs exhibits FM-like behavior with $T_c \sim 40$ K, while Thakur *et al*. [26] claimed that this compound is AFM with $T_N \sim 9$ K.

In order to understand how the magnetism of this compound is relevant to that of CuFeSb and Fe-based superconductors, we have grown $Cu_xFe_{1+y}As$ single crystals and characterize its composition, structure, electronic and magnetic properties. Our results show that this compound has a nonstoichiometric composition as expressed by $Cu_xFe_{1+y}As$ and is characterized by weak FM behavior with $T_c \sim 42$ K. This ferromagnetism fits into Yin *et al*'s model [7] as well due to its larger anion height ($Z_{As} \sim 1.80$ Å). Moreover, we also investigated Co doping effect on magnetic properties of $Cu_xFe_{1+y}As$ and found that Co doping enhances the ferromagnetism of $Cu_xFe_{1+y}As$. This result, together with the fact of relatively low T_c in $Cu_xFe_{1+y}As$, suggests that the ferromagnetism of this material depends not only on the anion height, but also on carrier density and itinerancy.

II. EXPERIMENT

We have synthesized both polycrystalline and single crystal $Cu_xFe_{1+y}As$ samples using the stoichiometric ratio CuFeAs. The polycrystalline sample was prepared with starting materials of FeAs and Cu powder using a traditional solid state reaction method. The precursor FeAs was prepared using the method reported in ref. [26]. The thoroughly mixed powder of FeAs and Cu

with the FeAs:Cu ratio of 1:1 was pelletized, sealed in an evacuated quartz tube and sintered first at 700 °C for 12 h and then at 1065 °C for 24 h, followed by cooling with a rate of 70 °C/h in the 1065-300°C range. The single crystal growth of $Cu_xFe_{1+y}As$ followed a similar procedure except that we used a different cooling process: the sample was first cooled with a rate of 1 °C/h from 1130 °C to 900°C and then followed by natural cooling with the furnace being turned off. We can easily obtain crystals with the lateral dimension of 1-2 mm and the thickness of 0.2-0.5 mm using this FeAs self-flux method. The inset in Fig. 2 shows an image of a typical crystal. As we will show below, the actual compositions of polycrystalline and single crystal samples involve nonstoichiometry for both Cu and Fe. Therefore, we use the $Cu_xFe_{1+y}As$ formulae to represent this compound as we did above. Moreover, we also prepared Co-doped polycrystalline samples with the nominal compositions of $CuFe_{1-z}Co_zAs$ (z = 0.1, 0.2, 0.3, 0.4 and 0.5) using the conditions similar to those used for $Cu_xFe_{1+y}As$ polycrystalline synthesis. Like $Cu_xFe_{1+y}As$, these samples also have actual compositions differing from their nominal compositions, which will be discussed in detail below. The composition analyses suggest that Co is indeed doped into Fe sites as we expected. The single crystal growth effort was not successful for any Co-doped samples.

The structures of our synthesized materials are characterized using a powder x-ray diffractometer with Cu Kα radiation (Rigaku D/max2200PC). The sample compositions were analyzed using energy dispersive x-ray spectrometer (EDXS). The magnetic properties of the samples were measured using the Quantum Design SQUID magnetometer. The resistivity measurements were conducted using a standard four-probe method in a Physical Property Measurement System (PPMS, Quantum Design). For CuFeAs single crystals, we also measured its specific heat using the adiabatic thermal relaxation technique in the PPMS.

III. RESULTS AND DISCUSSIONS

A. $Cu_xFe_{1+y}As$

Our x-ray diffraction analyses show that our synthesized $Cu_xFe_{1+y}As$ crystallizes in Cu_2Sb-type tetragonal structure with space group *P4*/*nmm*, consistent with the results reported by

by Lv [25] and Thakur *et al*. [26]. Figure 1a shows the room-temperature powder X-ray diffraction (XRD) pattern of $Cu_xFe_{1+y}As$ polycrystalline sample collected using a step mode with 8s per step. In this sample, in addition to the major $Cu_xFe_{1+y}As$ phase, we also observed two minor impurity phases, *i.e*. Cu_3As and FeAs. We performed Rietveld refinement of the XRD data shown in Fig. 1 using the General Structure Analysis System (GSAS) code and the two impurity phases were included in the refinement. The content of impurity phase estimated from the refinement is 3.93% for Cu_3As and 4.41% for FeAs. The refined structure is shown in Fig. 1b and the structural parameters derived from the refinement, including the lattice parameters, bonding length and angles and atomic positions in the unit cell are given in Table 1. Overall, $Cu_xFe_{1+y}As$ share a similar structure with LiFeAs and CuFeSb, as revealed in previous work [25-26]. Fe and As (or Sb) form anti-PbO-type layers in all these materials. Most structural parameters of $Cu_xFe_{1+y}As$ are closer to those of CuFeSb we previously reported. First, the Fe-As bonding length in $Cu_xFe_{1+y}As$ is 2.5986(12) Å, slightly smaller than the Fe-Sb bonding length (2.693(1)Å) in CuFeSb [24], but much greater than the Fe-As length (2.414 Å) in LiFeAs [23, 27-28]. Second, the As-Fe-As bonding angles α and β (see Fig. 1b for the definitions of α and β) are 92.15(5)° and 118.765(31)° respectively, ~1.7°/1° different from α (=93.860(5)°) and β (=117.793(3)°) in CuFeSb [24], but ~11°/6° differing from α (=102.87°) and β (=112.86°) in LiFeAs [23, 27-28]. From the schematic of structure in Fig. 1b, it can be seen that the As height Z_{As} from the Fe plane can be estimated from the Fe-As bonding length and the bonding angle α. The Z_{As} we determined for $Cu_xFe_{1+y}As$ is ~1.80 Å, which is slightly smaller than the Sb height from the Fe plane in CuFeSb (Z_{Sb} = 1.84 Å) [24], but much greater than Z_{As} in other iron pnictides (Z_{As} = 1.51 Å for LiFeAs [23], 1.31 Å for LaOFeAs [11], 1.35 Å for $BaFe_2As_2$ [12]) or Z_{Se}/Z_{Te} in iron chalcogenides (Z_{Se} = 1.47 Å for $Fe_{1.01}Se$ [29]; Z_{Te} = 1.77 Å for $Fe_{1+y}Te$ [18]). We note that the Z_{As} determined by Thakur *et al*. [26] for $Cu_xFe_{1+y}As$ is 1.74 Å, smaller than our determined value. This may be attributed to the difference in composition between our samples and theirs. As we show below, Cu nonstoichiometry may be responsible for the sample composition and structure variations. Another structural characteristic of $Cu_xFe_{1+y}As$ is that its lattice parameter c (=5.92116(20)Å) is much smaller than that of CuFeSb (c = 6.25152(4) Å) and those of other iron pnictides (*e.g*. c = 6.3534 Å for LiFeAs [23]). This is also observed by Thakur *et al.* [26] (c = 5.8925(4) Å).

Figure 2 shows the XRD pattern of the (00*l*) plane for a $Cu_xFe_{1+y}As$ single crystal. The sharp (00*l*) diffraction peaks demonstrate the good quality of crystallization of our crystals. The lattice parameter *c* estimated from these (00*l*) diffraction peaks is 5.885(5) Å, slightly smaller than that obtained from the structural refinement (*c* = 5.92116(20) Å). We have also analyzed the composition of $Cu_xFe_{1+y}As$ single crystal samples using EDXS. Although the single crystals were prepared using the stoichiometric ratio of CuFeAs, the actual, averaged composition measured by the EDXS is $Cu_{0.62}Fe_{1.07}As$ (see Table 2), which implies that the Cu sites are not fully occupied and some Cu vacant sites are occupied by excessive Fe. For the polycrystalline sample, its measured composition is $Cu_{0.73}Fe_{0.99}As$, which has higher Cu concentration than single crystal samples, but hardly has excessive Fe occupying Cu sites. This result is more or less consistent with the composition estimated from the structure refinement, $Cu_{0.789}Fe_{0.947}As_{1.039}$ as shown in Table 1. The non-stoichiometric composition of $Cu_xFe_{1+y}As$ is in contrast with the stoichiometric composition of CuFeSb.

We characterized electronic and magnetic properties of $Cu_xFe_{1+y}As$ via magnetization, transport property and specific heat measurements. Figure 3a shows the magnetization as a function of temperature $M(T)$ for both polycrystalline and single crystal samples of $Cu_xFe_{1+y}As$. The isothermal magnetization $M(H)$ at 2K for these samples is presented in Fig. 3b. For the single crystal sample, we conducted measurements with the external magnetic field being applied along the *ab*-plane and *c*-axis respectively. The magnetic transition probed in $M(T)$, together with the magnetic polarization and hysteresis seen in $M(H)$, suggest the presence of weak FM behavior in $Cu_xFe_{1+y}As$, with the Curie temperature T_c being ~ 22 K for the polycrystalline sample and ~ 42 K for the single crystal sample [T_c is defined as the peak temperature of the derivative of magnetization, *i.e.* $-dM(T)/dT$]. The saturated moment at 2 K is ~ 0.33 μ_B/Fe for the polycrystalline sample, 0.28 μ_B/Fe for $H//ab$ and ~ 0.38 μ_B/Fe for $H//c$ for the single crystal sample. The small difference of saturated moment between the *ab*-plane and *c*-axis indicates a weak magnetic anisotropy; this is also confirmed by a small $M(H)$ hysteresis loop (see the inset in Fig. 3b). The ferromagnetism we observed in $Cu_xFe_{1+y}As$ is much weaker than the ferromagnetism in CuFeSb where the FM ordering temperature T_c is ~ 375 K and the

saturated moment at 2 K is 1.7 μ_B/Fe [24]. The difference of T_c between the polycrystalline and single crystal samples is likely associated with Cu nonstoichiometry as discussed below.

Our observation of weak ferromagnetism in $Cu_xFe_{1+y}As$ is consistent with the FM-like behavior with $T_c \sim 40$ K previously observed by Lv *et al*. in a polycrystalline sample [25]. However, Thahur *et al*. [26] argued that CuFeAs is AFM with $T_N \sim 9$ K at zero or low fields but becomes FM when the applied magnetic field is increased above 500 Oe. Their argument was based on the observation that their $M(T)$ data at low fields exhibit a cusp-like feature at lower fields and $M(H)$ displays a linear field dependence in the <200 Oe lower field range. We indeed observed similar features in our samples. For instance, as shown in the inset of Fig. 3a, the $M(T)$ data collected at 100 Oe for the polycrystalline sample shows a clear cusp-like feature near 10 K. However, we do not think this feature corresponds to an AFM transition for several reasons. Firstly, the temperature and field dependences of magnetizations we presented above for $Cu_xFe_{1+y}As$ single crystals are quite consistent weak ferromagnetism. Secondly, as shown in Fig.3a, we did not observe significant anisotropy in $M(T)$ between $H//ab$ and $H//c$, which is usually expected for an AFM state. The cusp-like feature in $M(T)$ measured under a small field can be attributed to the fact that weakly polarized FM domains leads to partial magnetization cancelation between domains. The linear increase of magnetization with field in a low field range (<200 Oe) should originate from weak FM domain polarization and/or magnetic response of the impurity phases such as FeAs and Cu_3As. Although we disagree with Thahur *et al*'s argument of antiferromagnetism, we cannot exclude the possibility that our observed weak FM behavior in $Cu_xFe_{1+y}As$ is from a FM component of a canted AFM state or from a ferrimagnetic state. Detailed neutron scattering measurements are necessarily required to clarify this issue.

Figure 4a presents the in-plane and out-of-plane resistivity (ρ_{ab}, ρ_c) as a function of temperature for $Cu_xFe_{1+y}As$ single crystal samples. ρ_{ab} and ρ_c exhibit an anisotropy consist with the layered structure character of $Cu_xFe_{1+y}As$, with $\rho_c/\rho_{ab} \sim 8.2$ at 2 K. While ρ_{ab} displays metallic behavior in the whole temperature range and follows T^2 temperature dependence for $T <$ 10 K (see the inset of Fig. 4a), ρ_c shows a crossover from non-metallic-to-metallic behavior near 20K. The anisotropic properties between ρ_c and ρ_{ab} imply that the FS of $Cu_xFe_{1+y}As$ has quasi-

two-dimensional (2D) nature, consistent with the quasi-2D characteristic of FS observed in iron pnictides [30-34] and chalcogenides [21-22]. We note that LiFeAs also exhibits a nonmetal-to-metal crossover in ρ_c; but this crossover occurs at a much higher temperature (~ 250 K) as compared to $Cu_xFe_{1+y}As$. This indicates that the FS of $Cu_xFe_{1+y}As$ shows greater electronic anisotropy than that of LiFeAs though they share similar layered structure. LiFeAs is known as having strong electron-electron scattering at low temperature, as reflected in the quadratic temperature dependence of resistivity [35]. Our observation of $\rho_{ab} \propto T^2$ for $T < 10$K suggests that the electron-electron scattering is also strong in $Cu_xFe_{1+y}As$. Strong electron-electron scattering is usually accompanied with other strong correlation effect such as large effective mass of quasi-particles. To verify this, we measured low temperature specific heat of a $Cu_xFe_{1+y}As$ single crystal sample. The results of measurements are presented in Fig. 5. In the inset of Fig. 5, we show the specific heat data below 5 K can be fitted to $c = \gamma T + \beta T^3$, where γT and βT^3 represent electronic and phonon specific heat respectively. The Somerfield coefficient γ estimated from this fit is ~ 40.0 mJ/(mol K^2), much larger than that of LiFeAs (γ = 8.5 mJ/mol K^2) [36]. Such a large γ value renders $Cu_xFe_{1+y}As$ a strongly correlated material. It is also worth noting that we did not observe specific heat anomaly at T_c ~ 42 K. This might be attributed to the fact that the ferromagnetism in $Cu_xFe_{1+y}As$ is weak. A similar absence of specific heat anomaly at T_c is also observed in weak FM material $Yb_xFe_4Sb_{12}$[37]. To evaluate the contribution of ferromagnetism to specific heat, we have also fitted the low temperature specific data to $C = \gamma T + \beta T^3 + \alpha T^{1.5}$, with the $\alpha T^{1.5}$ term representing the contribution from ferromagnetism. Nevertheless, the magnetic contribution to specific heat is found to be negligibly small, consistent with the absence of specific heat anomaly at T_c.

B. Co-doped $Cu_xFe_{1+y}As$

Given that charge carrier doping into iron pnictides and chalcogenides parent compounds can suppress their AFM ordering and induce superconductivity, a natural question is how the weak ferromagnetism in $Cu_xFe_{1+y}As$ responds to charge carrier doping. Clarification of this question is apparently instrumental to the understanding of the magnetism of Fe-based superconductor parent compounds. To address this issue, we have studied Co doping effect on

the ferromagnetism of $Cu_xFe_{1+y}As$. Figure 6 shows powder XRD patterns of Co-doped samples, $CuFe_{1-z}Co_zAs$ (z = 0.1, 0.3 and 0.4). All doped samples show impurity phases of FeAs and Cu_3As as the $Cu_xFe_{1+y}As$ polycrystalline sample does. Although the structure of the major $Cu_xFe_{1+y}As$ phase remains tetragonal in the z = 0-0.5 doping range, lattice parameters a and c gradually decrease with the increase of Co concentration, with $\Delta a/a$ = -0.51% and $\Delta c/c$ = -1.0% for z(Co) = 0.5 (see Fig. 7). Such structural changes may be understood in terms of the difference in ionic radius between Co, Fe and Cu. The possible chemical valence of Co is 3+ and its ionic radius is 0.63 Å, smaller than the ionic radii of Fe^{2+} (0.74 Å) and Cu^{1+} (0.96 Å). Thus, no matter whether Co occupies Fe or Cu sites, smaller lattice parameters could be expected.

To determine whether Co occupies Fe or Cu sites, we have analyzed the compositions of the Co-doped samples using EDXS. Table 2 displays comparison between the nominal and the measured compositions for the Co-doped samples. From the measured compositions, we found that with the increase of Co concentration, the Cu content remains unchanged with x(Cu) ~ 0.76, while the Fe content decreases, with the total content of Fe and Co being close to 100%. These facts suggest that dopant Co occupies the Fe sites on the Fe plane. We did not include the data for z(Co) =0.4 and 0.5 samples, since they contain too much impurity phases.

Figure 8a shows the temperature dependence of magnetization for polycrystalline $Cu_xFe_{1-z}Co_zAs$. It can be clearly seen that Co doping enhances the ferromagnetism of $Cu_xFe_{1+y}As$ with T_c increasing from ~ 22 K for z = 0 to ~ 83 K for z = 0.5. However, the saturated moment is decreased from ~ 0.4 μ_B/Fe for z =0 to ~ 0.2 μ_B/Fe for z = 0.5 (Fig. 8b) in spite of T_c increase. This is probably caused by the suppression of carrier itinerancy due to disorder scattering as shown below. We present the normalized resistivity data of $CuFe_{1-z}Co_zAs$ in Fig. 9. All the samples of this series remain metallic in the whole temperature range. However, the metallicity gradually weakens with the increase of Co concentration, which is manifested in the variation of the ratio of room-temperature resistivity to residual resistivity (RRR) with Co concentration. RRR is ~ 3.2 for the undoped sample, but decreases to ~ 1.7 for z(Co) = 0.5. The resistivity data for each sample shown in Fig. 9 also show a kink near 220 K. This feature is likely caused by the impurity phase Cu_3As which is known to have a resistivity anomaly near 220K [38-39].

Next let's first discuss the origin of the ferromagnetism of $Cu_xFe_{1+y}As$. Given that $Cu_xFe_{1+y}As$ is structurally similar to CuFeSb as discussed above, the weak ferromagnetism in these two materials may have similar mechanism. For CuFeSb, we previously argued that the large height of Sb from the Fe-plane plays a key role in achieving ferromagnetism. We discussed two possible scenarios in which large anion height Z_{Sb} favors FM coupling. Firstly, the large Z_{Sb} could lead the coupling between the Fe t_{2g} states and the Sb 5p states to become weak. The first principles calculations show that weakening of such Fe t_{2g}-Sb 5p coupling increases the density of states at the Fermi level, $N(E_F)$ [2]. High $N(E_F)$ can trigger itinerant ferromagnetism according to Stoner criterion. Secondly, the ferromagnetism of CuFeSb can find interpretation from the unified microscopic model proposed by Yin *et al.* [7] which assumes that in iron pnictides/chalcogenides there exits competition between the AFM superexchange interaction of localized moments and the FM interaction mediated by the Hund's rule coupling between localized spins and itinerant electrons. Such competing AFM and FM magnetic interactions are tuned by the anion height. The large anion height favors ferromagnetism, since the AFM superexchange interaction occurs via the anions and would naturally become weak when the anions are further away from the Fe-plane.

Since the As height from the Fe-plane in $Cu_xFe_{1+y}As$ is ~1.80 Å, slightly smaller than the Z_{Sb} (=1.84 Å) of CuFeSb, we may anticipate both mechanisms of ferromagnetism discussed above may be applicable to $Cu_xFe_{1+y}As$. However, one may ask why $Cu_xFe_{1+y}As$ has a T_c (~ 22-42K, see Fig.3a) much lower than that of CuFeSb (T_c ~ 375K). The difference in electronic band structures between these two materials may give an answer to this question. In general, the Curie temperature of a FM material should be dependent on specific characteristics of electronic band structure regardless of its FM origin. Although energy band structures of CuFeSb and $Cu_xFe_{1+y}As$ have not been reported, we can reasonably expect large difference between them. As indicated above, CuFeSb has a stoichiometric composition with both Cu and Fe sites being fully occupied, whereas $Cu_xFe_{1+y}As$ is nonstoichiometric with Cu sites being partially vacant (see Table 2). The fact that the different compositions between the polycrystalline ($Cu_{0.73}Fe_{0.99}As$) and single crystal ($Cu_{0.62}Fe_{1.07}As$) samples result in distinct T_c (~ 22 K for the polycrystalline

sample and ~ 42 K for the single crystal sample), indeed implies that the FM coupling in $Cu_xFe_{1+y}As$ depends on Cu concentration and the electronic state near the Fermi level may involve contributions from Cu 3d orbitals. Under this circumstance, the vacancies of Cu sites in $Cu_xFe_{1+y}As$ would cause heavy hole doping, which might be responsible for its lower T_c.

The Co doping effect described above provides further support for this argument. As indicated above, Co is doped into Fe sites. Substitution of Co^{3+} for Fe^{2+} should cause electron doping. Given that hole doping reduces T_c as suggested above, the electron doping induced by Co doping would be naturally expected to increase T_c. The reduction of saturated moment caused by Co doping (Fig. 8b) may be caused by disorders induced by doping. Further verification of these interpretations requires electronic band structure calculations and photoemission spectroscopy measurements for CuFeSb and $Cu_xFe_{1+y}As$. Another possibility of weak ferromagnetism in $Cu_xFe_{1+y}As$ might be either from a FM component of a canted AFM state or a ferrimagnetic state; detailed neutron scattering studies on $Cu_xFe_{1+y}As$ single crystals are necessary to elucidate to this issue, as indicated above.

The presence of ferromagnetism in $Cu_xFe_{1+y}As$ and CuFeSb supports the idea that iron pnictides and chalcogenides involves competition between AFM and FM correlations and a large anion height favors the ferromagnetism [7-8]. However, the anion height may not be the only parameter which can stabilize ferromagnetism in iron pnictides/charcogenides. We note FM correlations can also be enhanced through controlling other parameters such as pressure and chemical composition in iron chalcogenide/pnictide systems. One remarkable example is that hydrostatic pressure can tune $Fe_{1.03}Te$ from a AFM to a FM state [40]. The other important example is that FM fluctuations are observed in overdoped $Li_{1-y}Fe_{1+y}As$ though pristine LiFeAs exhibits AFM fluctuations [41]. These experimental facts clearly indicate that band structure tuning by pressure or chemical doping can also bring the system close to a FM instability in iron pnictides/chalcogenides.

IV. CONCLUSIONS

In summary, we have grown $Cu_xFe_{1+y}As$ single crystals and characterized its electronic and magnetic properties through electronic transport, magnetization and specific heat measurements. Although this compound shares a similar tetragonal structure with superconductor LiFeAs/NaFeAs, it exhibits weak FM behavior, with T_c depending on Cu concentration (~22-42K). Its electronic ground state behaves like a Fermi liquid state with a relatively large Sommerfeld coefficient $\gamma \sim 40$ mJ/(mol K^2). Like CuFeSb, $Cu_xFe_{1+y}As$ has a large anion height (Z_{As} ~1.80 Å). This provides an additional support for the theoretical proposal that iron pnictides and chalcogenides involve competing magnetic interactions and the large anion height favors FM correlations. The fact that the T_c of $Cu_xFe_{1+y}As$ is much lower than that of CuFeSb ($T_c \sim 375$ K) can probably be attributed to heavy hole doping caused by Cu nonstoichiometry. The FM enhancement caused by Co doping provides strong support for this argument.

ACKNOELEDGEMENTS

We would like to acknowledge informative discussions with W. Yin. This work was supported by National Natural Science Foundation of China (11374043, 11174043, 51371004), Natural Science Foundation of Jiangsu Educational Department (13KJA430001), six-talent peak of Jiangsu Province (2011-XCL-022 and 2012-XCL- 036), and Jiangsu Innovation Project for Undergraduate Student. The work at Tulane is supported by the DOE under grant DE-SC0012432. X. K. acknowledges support from the start-up funds at Michigan State University.

∗ njqb@cslg.edu.cn; zmao@tulane.edu

References:

1 J. Wu, P. Phillips and A. H. C. Neto, *Phys. Rev. Lett* **101**, 126401-4 (2008)

2 F. Ma, Z.-Y. Lu and T. Xiang, *Phys. Rev. B* **78**, 224517 (2008)

3 Q. Si and E. Abrahams, *Phys. Rev. Lett.* **101**, 076401 (2008)

4 T. Yildirim, *Phys. Rev. Lett.* **101**, 057010 (2008)

[5] F. Ma, W. Ji, J. Hu, Z.-Y. Lu and T. Xiang, *Phys. Rev. Lett.* **102**, 177003-4 (2009)

[6] M. D. Johannes and I. I. Mazin, *Phys. Rev. B* **79**, 220510 (2009)

[7] W.-G. Yin, C.-C. Lee and W. Ku, *Phys. Rev. Lett.* **105**, 107004 (2010)

[8] C.-Y. Moon and H. J. Choi, *Phys. Rev. Lett.* **104**, 057003 (2010)

[9] J. Hu, B. Xu, W. Liu, N.-N. Hao and Y. Wang, *Phys. Rev. B* **85**, 144403 (2012)

[10] J. Hu and H. Ding, *Sci. Rep.* **2**, 381 (2012)

[11] C. de la Cruz, Q. Huang, J. W. Lynn, J. Li, W. R. Ii, J. L. Zarestky, H. A. Mook, G. F. Chen, J. L. Luo, N. L. Wang and P. Dai, *Nature* **453**, 899-902 (2008)

[12] Q. Huang, Y. Qiu, W. Bao, M. A. Green, J. W. Lynn, Y. C. Gasparovic, T. Wu, G. Wu and X. H. Chen, *Phys. Rev. Lett* **101**, 257003 (2008)

[13] J. Dong, H. J. Zhang, G. Xu, Z. Li, G. Li, W. Z. Hu, D. Wu, G. F. Chen, X. Dai, J. L. Luo, Z. Fang and N. L. Wang, *Europhys. Lett.* **83**, 27006 (2008)

[14] D. J. Singh, *Phys. Rev. B* **78**, 094511 (2008)

[15] F. Ma and Z.-Y. Lu, *Phys. Rev. B* **78**, 033111 (2008)

[16] V. Cvetkovic and Z. Tesanovic, *Europhys. Lett.* **85**, 37002 (2009)

[17] I. I. Mazin, *Nature* **464**, 183-186 (2010)

[18] W. Bao, Y. Qiu, Q. Huang, M. A. Green, P. Zajdel, M. R. Fitzsimmons, M. Zhernenkov, S. Chang, M. Fang, B. Qian, E. K. Vehstedt, J. Yang, H. M. Pham, L. Spinu and Z. Q. Mao, *Phys. Rev. Lett* **102**, 247001-4 (2009)

[19] S. Li, C. de la Cruz, Q. Huang, Y. Chen, J. W. Lynn, J. Hu, Y.-L. Huang, F.-C. Hsu, K.-W. Yeh, M.-K. Wu and P. Dai, *Physical Review B (Condensed Matter and Materials Physics)* **79**, 054503-7 (2009)

[20] A. Subedi, L. J. Zhang, D. J. Singh and M. H. Du, *Phys. Rev. B* **78**, 134514 (2008)

[21] Y. Xia, D. Qian, L. Wray, D. Hsieh, G. F. Chen, J. L. Luo, N. L. Wang and M. Z. Hasan, *Phys. Rev. Lett.* **103**, 037002-4 (2009)

[22] Z. K. Liu, R. H. He, D. H. Lu, M. Yi, Y. L. Chen, M. Hashimoto, R. G. Moore, S. K. Mo, E. A. Nowadnick, J. Hu, T. J. Liu, Z. Q. Mao, T. P. Devereaux, Z. Hussain and Z. X. Shen, *Phys. Rev. Lett.* **110**, 037003 (2013)

[23] M. J. Pitcher, D. R. Parker, P. Adamson, S. J. C. Herkelrath, A. T. Boothroyd, R. M. Ibberson, M. Brunelli and S. J. Clarke, *Chem. Commun.* 5918-5920 (2008)

[24] B. Qian, J. Lee, J. Hu, G. C. Wang, P. Kumar, M. H. Fang, T. J. Liu, D. Fobes, H. Pham, L. Spinu, X. S. Wu, M. Green, S. H. Lee and Z. Q. Mao, *Phys. Rev. B* **85**, 144427 (2012)

[25] B. Lv. Syntheses, structures and properties of iron arsenic-based superconductors. University of Houston, 2009.

[26] G. S. Thakur, Z. Haque, L. C. Gupta and A. K. Ganguli, *J. Phys. Soc. Jpn.* **83**, 054706 (2014)

[27] W. Yao, D. Xiao and Q. Niu, *Phys. Rev. B* **77**, 235406 (2008)

[28] J. H. Tapp, Z. Tang, B. Lv, K. Sasmal, B. Lorenz, P. C. W. Chu and A. M. Guloy, *Phys. Rev. B* **78**, 060505 (2008)

[29] T. M. McQueen, Q. Huang, V. Ksenofontov, C. Felser, Q. Xu, H. Zandbergen, Y. S. Hor, J. Allred, A. J. Williams, D. Qu, J. Checkelsky, N. P. Ong and R. J. Cava, *Phys. Rev. B* **79**, 014522-7 (2009)

[30] H. Ding, P. Richard, K. Nakayama, K. Sugawara, T. Arakane, Y. Sekiba, A. Takayama, S. Souma, T. Sato, T. Takahashi, Z. Wang, X. Dai, Z. Fang, G. F. Chen, J. L. Luo and N. L. Wang, *Europhys. Lett.* **83**, 47001 (2008)

[31] D. H. Lu, M. Yi, S. K. Mo, A. S. Erickson, J. Analytis, J. H. Chu, D. J. Singh, Z. Hussain, T. H. Geballe, I. R. Fisher and Z. X. Shen, *Nature* **455**, 81-84 (2008)

[32] C. Liu, G. D. Samolyuk, Y. Lee, N. Ni, T. Kondo, A. F. Santander-Syro, S. L. Bud'ko, J. L. McChesney, E. Rotenberg, T. Valla, A. V. Fedorov, P. C. Canfield, B. N. Harmon and A. Kaminski, *Phys. Rev. Lett.* **101**, 177005 (2008)

[33] V. B. Zabolotnyy, D. S. Inosov, D. V. Evtushinsky, A. Koitzsch, A. A. Kordyuk, G. L. Sun, J. T. Park, D. Haug, V. Hinkov, A. V. Boris, C. T. Lin, M. Knupfer, A. N. Yaresko, B. Buchner, A. Varykhalov, R. Follath and S. V. Borisenko, *Nature* **457**, 569-572 (2009)

[34] D. H. Lu, M. Yi, S. K. Mo, J. G. Analytis, J. H. Chu, A. S. Erickson, D. J. Singh, Z. Hussain, T. H. Geballe, I. R. Fisher and Z. X. Shen, *Physica C* **469**, 452-458 (2009)

[35] O. Heyer, T. Lorenz, V. B. Zabolotnyy, D. V. Evtushinsky, S. V. Borisenko, I. Morozov, L. Harnagea, S. Wurmehl, C. Hess and B. Büchner, *Phys. Rev. B* **84**, 064512 (2011)

[36] U. Stockert, M. Abdel-Hafiez, D. V. Evtushinsky, V. B. Zabolotnyy, A. U. B. Wolter, S. Wurmehl, I. Morozov, R. Klingeler, S. V. Borisenko and B. Büchner, *Phys. Rev. B* **83**, 224512 (2011)

[37] T. Ikeno, A. Mitsuda, T. Mizushima, T. Kuwai, Y. Isikawa and I. Tamura, *J. Phys. Soc. Jpn.* **76**, 024708 (2007)

[38] B. B. Begaev, A. V. Dooglav, V. P. Kal'chev, E. V. Krjukov, I. R. Mukhamedshin and I. N. Pen'kov, *Appl. Magn. Reson.* **22**, 577-588 (2002)

[39] L. J. Pauwels, G. Maervoet and R. Vervaeke, *Z. Anorg. Allg. Chem.* **397**, 307-313 (1973)

[40] M. Bendele, A. Maisuradze, B. Roessli, S. N. Gvasaliya, E. Pomjakushina, S. Weyeneth, K. Conder, H. Keller and R. Khasanov, *Phys. Rev. B* **87**, 060409 (2013)

[41] A. E. Taylor, M. J. Pitcher, R. A. Ewings, T. G. Perring, S. J. Clarke and A. T. Boothroyd, *Phys. Rev. B* **83**, 220514 (2011)

TABLE I. Refined structure parameters for $Cu_xFe_{1+y}As$ at 300 K. The number in square brackets indicates the numbers of symmetry of equivalent bond lengths.

Space group *P4*/*nmm*, *a* = *b* = 3.74331(16) Å, *c* = 5.92116(20) Å						
		x	*y*	*z*	Occupancy	Wyckoff positions
Atom coordinates	Cu	0.25	0.25	0.72779(44)	0.789(4)	2c
	Fe	0.75	0.25	0	0.947(2)	2b
	As	0.25	0.25	0.30444(29)	1.039(3)	2c
Bond lengths (Å)	Fe-As [4] 2.5986(12)	Fe-Fe [4] 2.64692(12)	Cu-As [1] 2.5067(31)	Cu-As [4] 2.65379(25)		
Bond angles (°) As-Fe-As	α=92.15(5)	β=118.765(31)				

Table 2: Comparison of nominal and actual compositions for $Cu_xFe_{1+y}As$ and $Cu_x(Fe_{1-z}Co_z)As$.

	Nominal compositions	Actual compositions
$Cu_xFe_{1+y}As$	single crystal	$Cu_{0.62}Fe_{1.07}As$
	Polycrystalline	$Cu_{0.73}Fe_{0.99}As$
$CuFe_{1-z}Co_zAs$ polycrystalline	$CuFe_{0.9}Co_{0.1}As$	$Cu_{0.76}Fe_{0.87}Co_{0.10}As$
	$CuFe_{0.8}Co_{0.2}As$	$Cu_{0.76}Fe_{0.85}Co_{0.18}As$
	$CuFe_{0.7}Co_{0.3}As$	$Cu_{0.76}Fe_{0.76}Co_{0.25}As$

Figure captions:

Figure 1: (a) Powder XRD of $Cu_{1+x}Fe_yAs$. (b) Crystal structure of $Cu_xFe_{1+y}As$; α refers to the As-Fe-As bonding angle formed by two neighboring As ions lying above the Fe plane, while β denotes the As-Fe-As angle formed by one As ion lying above and one As below the Fe-plane.

Figure 2: (00*l*) XRD pattern of a $Cu_xFe_{1+y}As$ single crystal. Inset: an image of a typical $Cu_xFe_{1+y}As$ single crystal.

Figure 3: (a) Temperature dependence of magnetization for $Cu_xFe_{1+y}As$ polycrystalline and single crystal samples, measured under a magnetic field of 1000 Oe and zero-field-cooling (ZFC) and field-cooling histories (FC). Inset: temperature dependence of magnetization for $Cu_xFe_{1+y}As$ polycrystalline measured under a field of 100 Oe. (b) Isothermal magnetization at 2K for $Cu_xFe_{1+y}As$ polycrystalline and single crystal samples; the field was applied to the ab-plane and c-axis respectively for the single crystal sample. The inset in (b) shows the magnetization as a function of field in a small field range.

Figure 4: Temperature dependences of in-plane and out-of-plane resistivity for $Cu_xFe_{1+y}As$ single crystals. Inset shows the in-plane resistivity on the scale of T^2.

Figure 5: Specific heat divided by temperature C/T as a function of temperature for a $Cu_xFe_{1+y}As$ single crystal. Inset, C/T vs. T^2.

Figure 6: Powder XRD patterns of $Cu(Fe_{1-z}Co_z)As$ polycrystalline samples.

Figure 7: Lattice parameters as a function of Co concentration at room temperature for $Cu(Fe_{1-z}Co_z)As$.

Figure 8: (a) Temperature dependence of magnetization measured under a field of 100 Oe with ZFC and FC histories for $Cu(Fe_{1-z}Co_z)As$ polycrystalline samples. (b) Isothermal magnetization at 2K for $Cu(Fe_{1-z}Co_z)As$ polycrystalline samples.

Figure 9: Temperature dependence of normalized resistivity for $Cu(Fe_{1-z}Co_z)As$ polycrystalline samples.

Figure 1

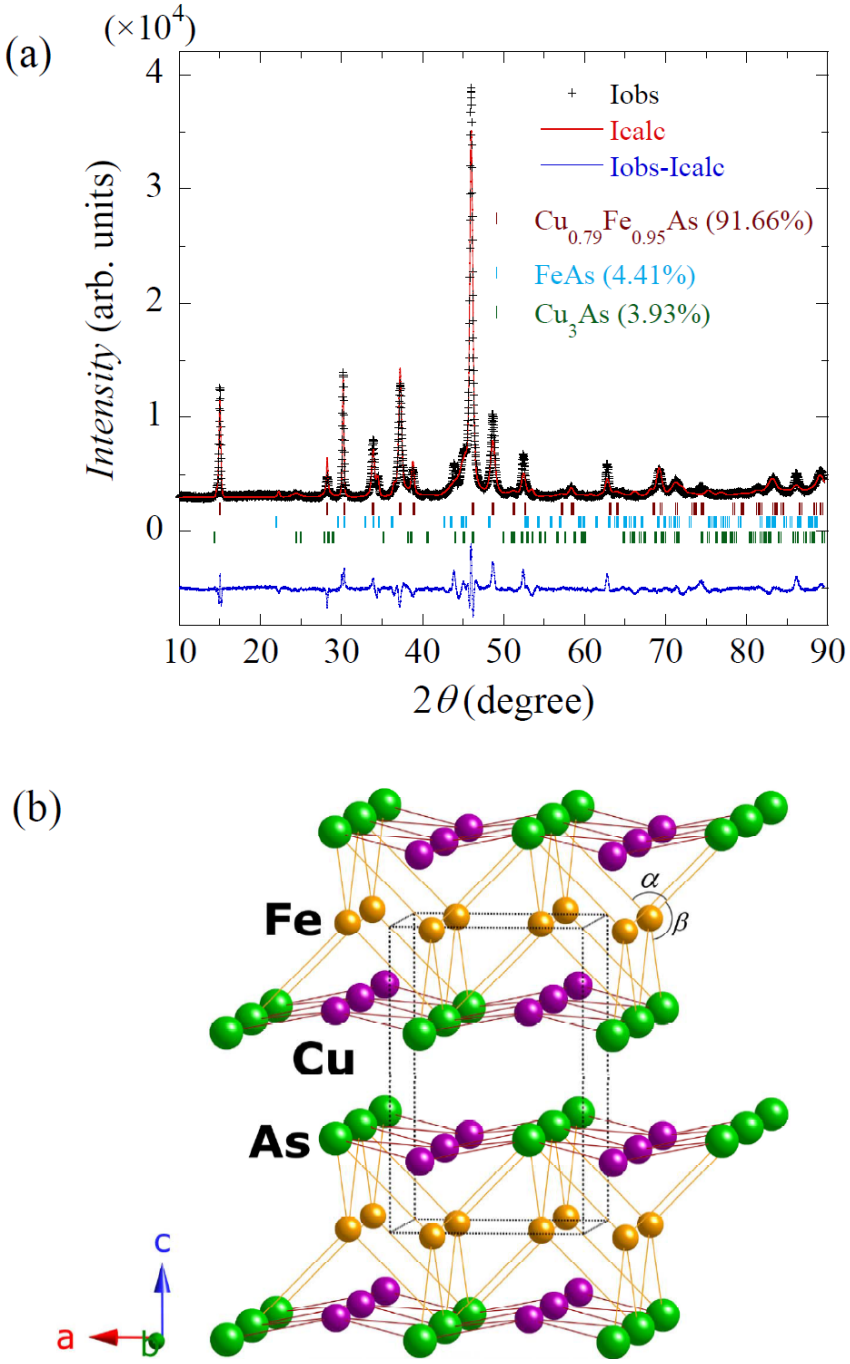
(a)
(×10^4)
Intensity (arb. units)
2θ (degree)
Iobs
Icalc
Iobs-Icalc
Cu0.79Fe0.95As (91.66%)
FeAs (4.41%)
Cu3As (3.93%)
(b)
Fe
Cu
As
α
β
c
a
b

Figure 2

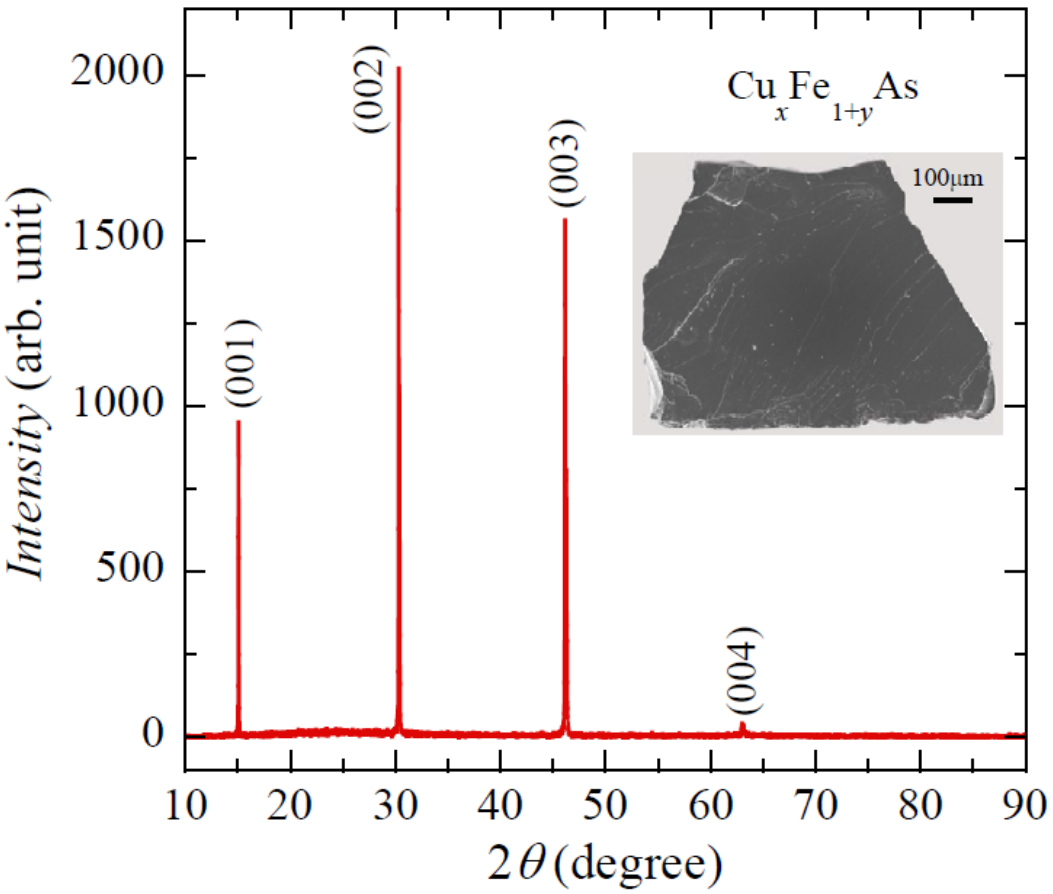
Cu x Fe 1+y As
100μm
(001)
(002)
(003)
(004)
Intensity (arb. unit)
2θ (degree)
0
500
1000
1500
2000
10
20
30
40
50
60
70
80
90

Figure 3

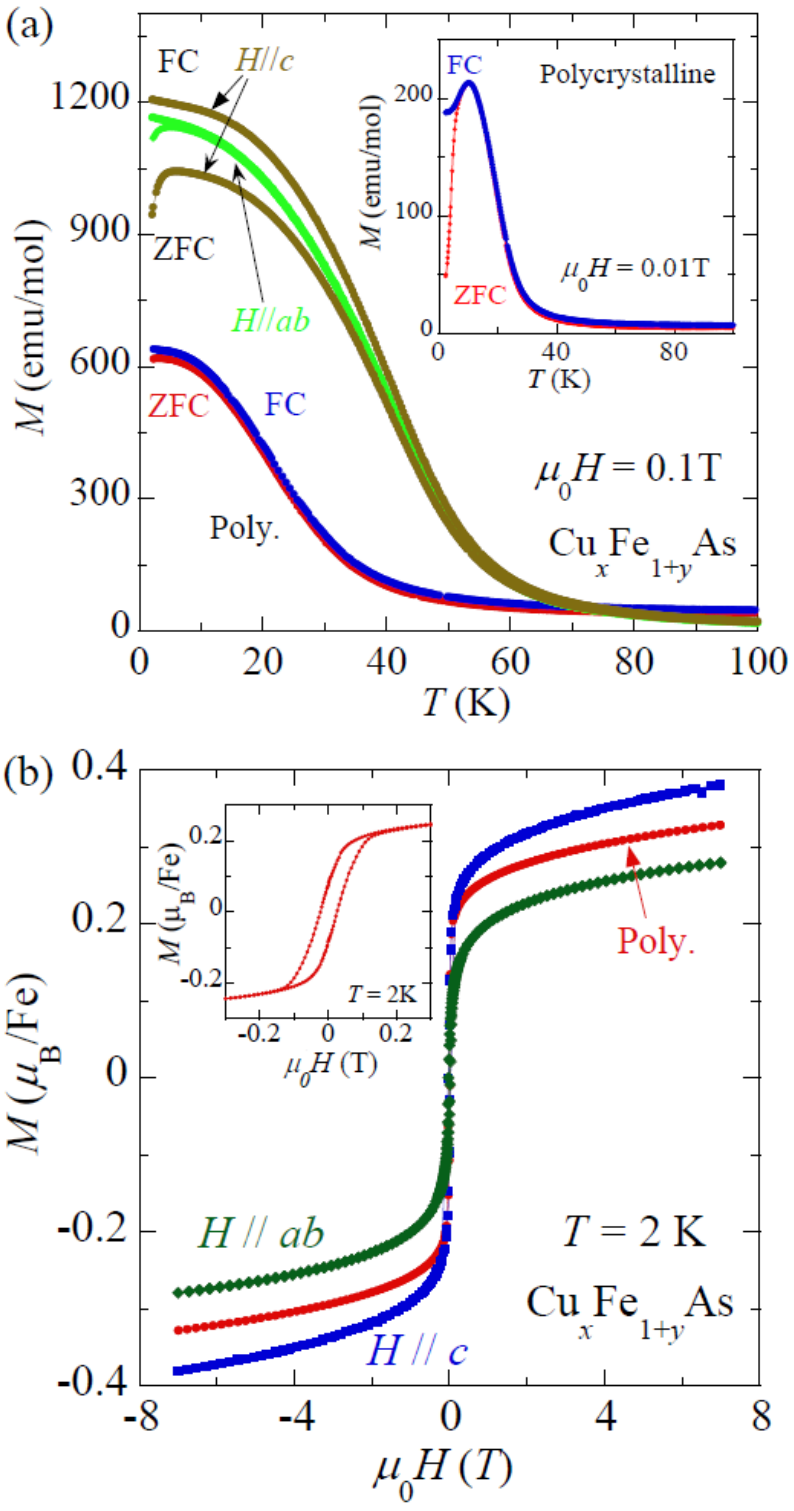
(a)
FC
H//c
ZFC
H//ab
ZFC
FC
Poly.
μ0H = 0.1T
Cu x Fe 1+y As
M (emu/mol)
T (K)
Polycrystalline
FC
ZFC
μ0H = 0.01T
M (emu/mol)
T (K)
(b)
Poly.
H // ab
H // c
T = 2 K
Cu x Fe 1+y As
M (μB/Fe)
μ0H (T)
T = 2K
M (μB/Fe)
μ0H (T)

Figure 4

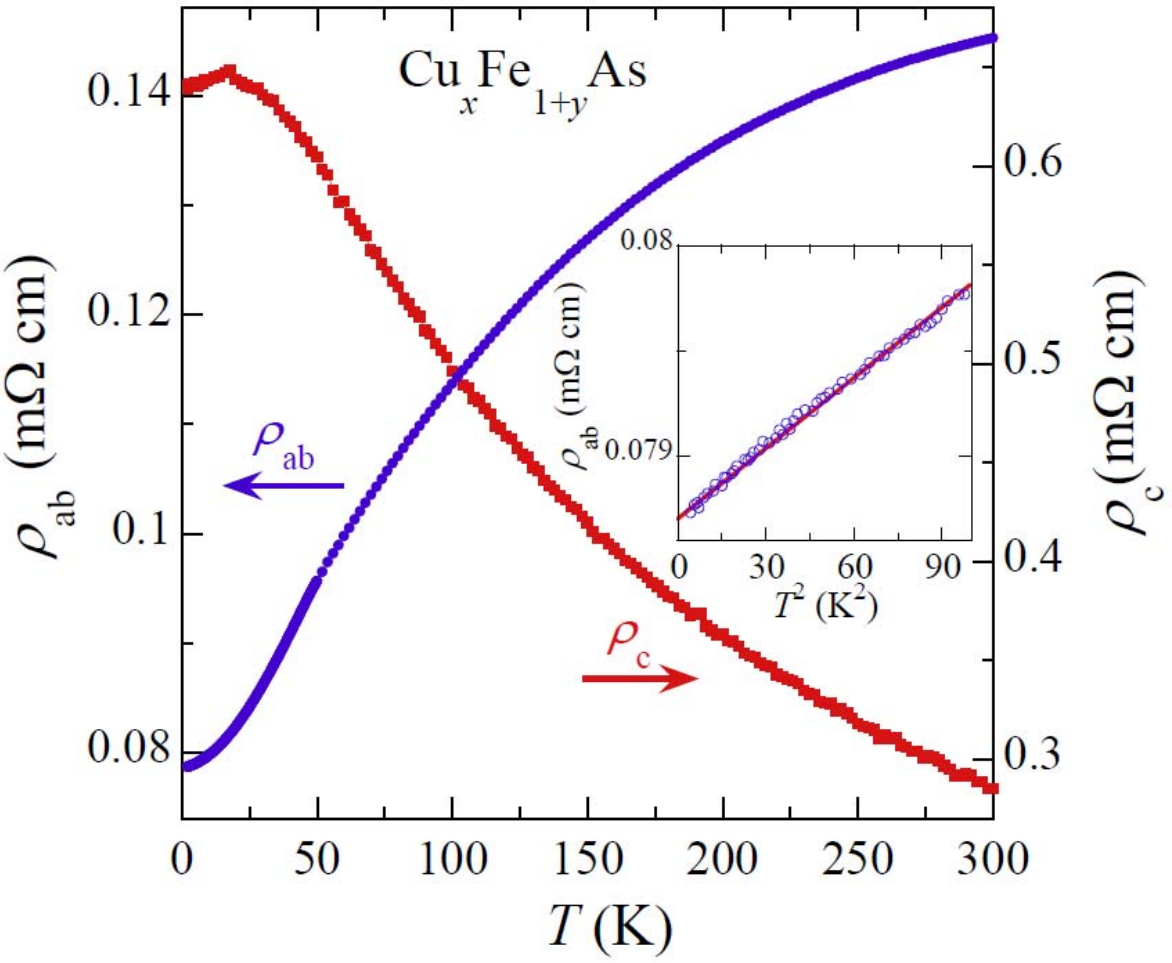
Cu x Fe 1+y As
0.14
0.12
0.1
0.08
0.6
0.5
0.4
0.3
0
50
100
150
200
250
300
T (K)
ρ ab (mΩ cm)
ρ c (mΩ cm)
ρ ab
ρ c
0.08
0.079
0
30
60
90
T 2 (K 2)
ρ ab (mΩ cm)

Figure 5

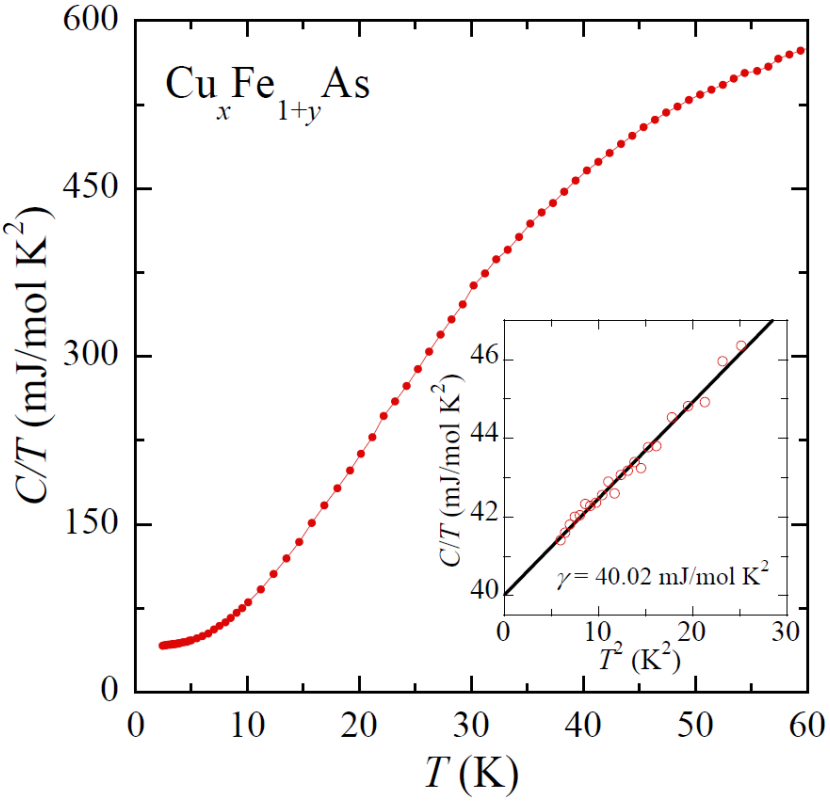
Cu x Fe 1+y As
C/T (mJ/mol K2)
T (K)
0
150
300
450
600
0
10
20
30
40
50
60
C/T (mJ/mol K2)
T2 (K2)
γ = 40.02 mJ/mol K2
40
42
44
46
0
10
20
30

Figure 6

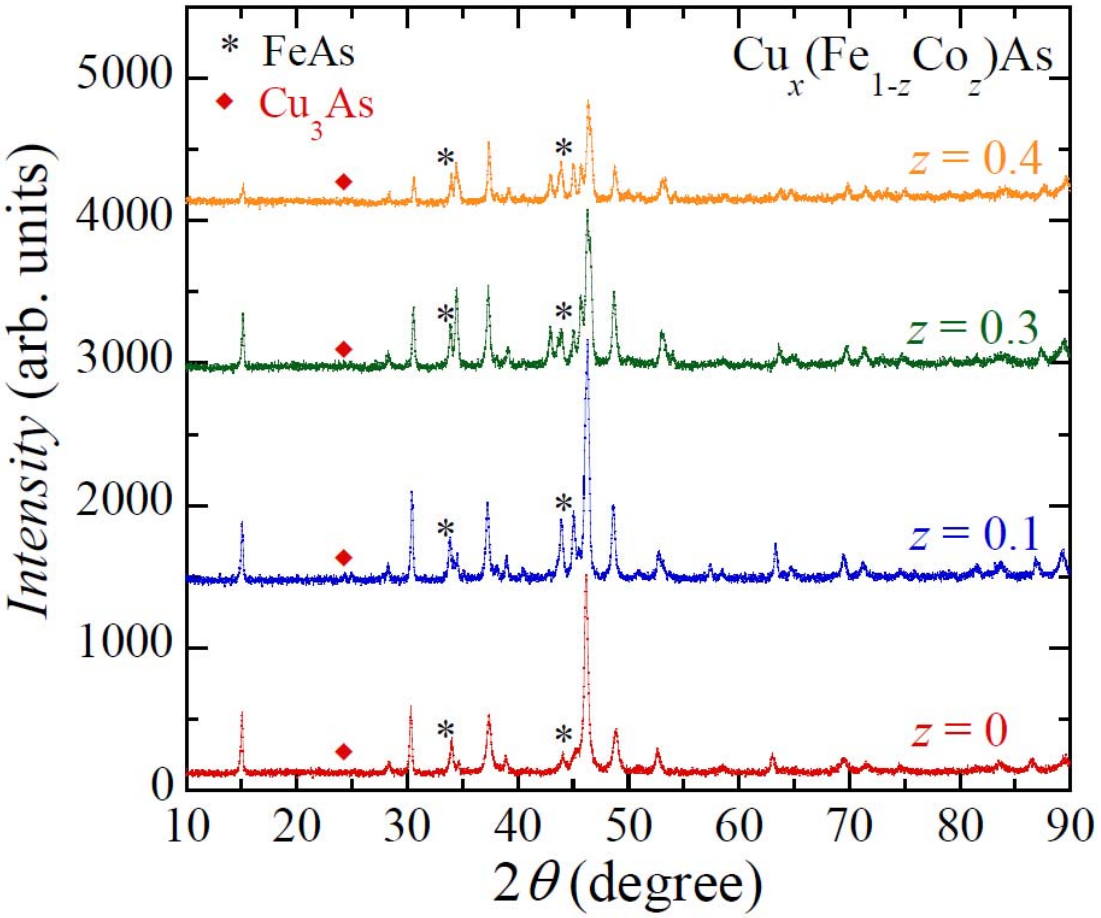
* FeAs
Cu3As
Cux(Fe1-zCoz)As
z = 0.4
z = 0.3
z = 0.1
z = 0
Intensity (arb. units)
2θ (degree)
0
1000
2000
3000
4000
5000
10
20
30
40
50
60
70
80
90

Figure 7

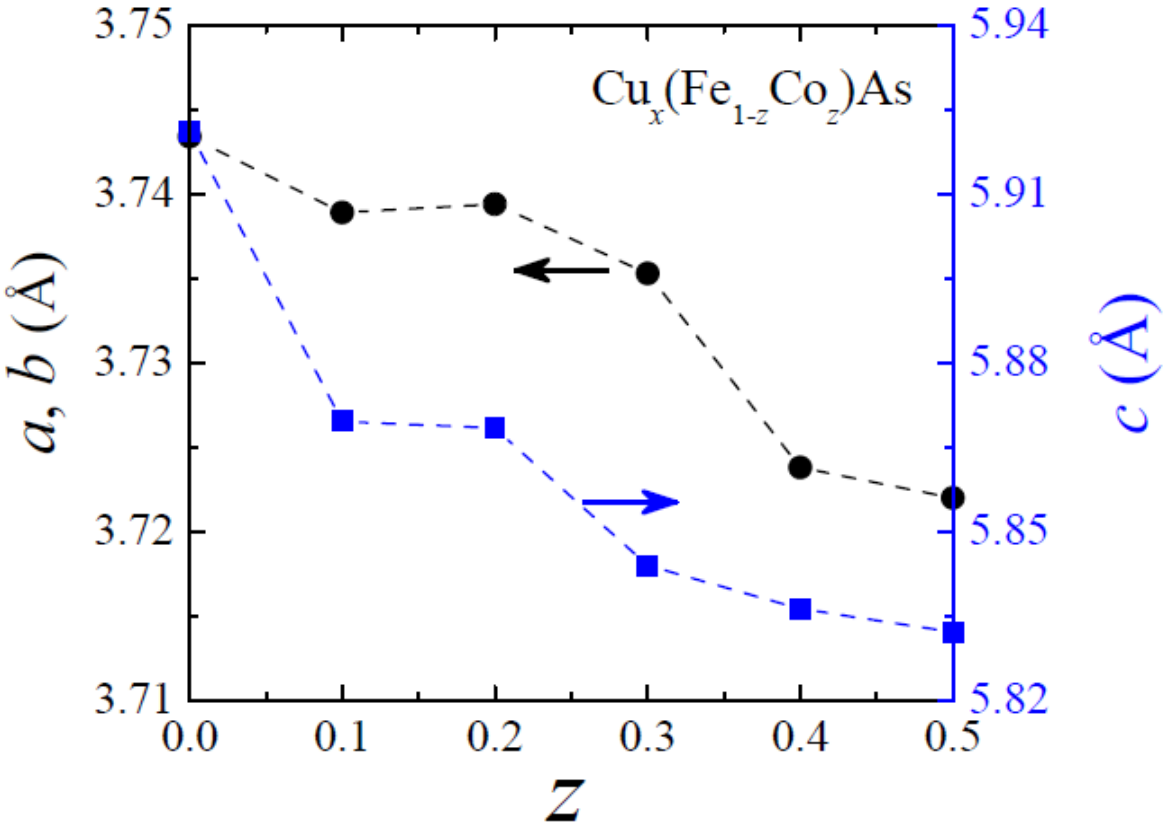
Cu$_x$(Fe$_{1-z}$Co$_z$)As
3.75
3.74
3.73
3.72
3.71
5.94
5.91
5.88
5.85
5.82
0.0
0.1
0.2
0.3
0.4
0.5
z
a, b (Å)
c (Å)

Figure 8

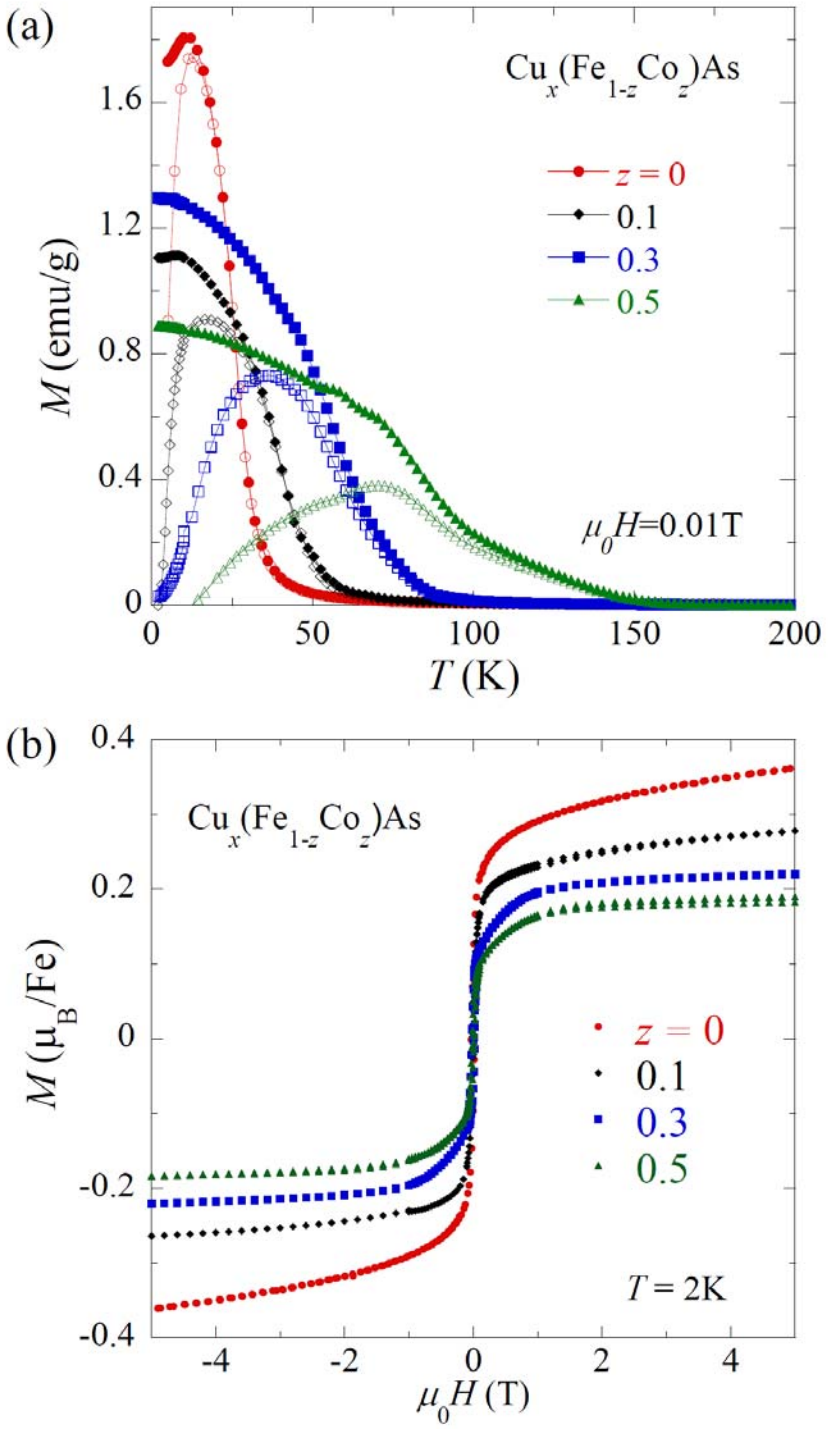
(a)
Cu$_x$(Fe$_{1-z}$Co$_z$)As
z = 0
0.1
0.3
0.5
$\mu_0 H$=0.01T
M (emu/g)
T (K)
(b)
Cu$_x$(Fe$_{1-z}$Co$_z$)As
z = 0
0.1
0.3
0.5
T = 2K
M (μ_B/Fe)
$\mu_0 H$ (T)

Figure 9

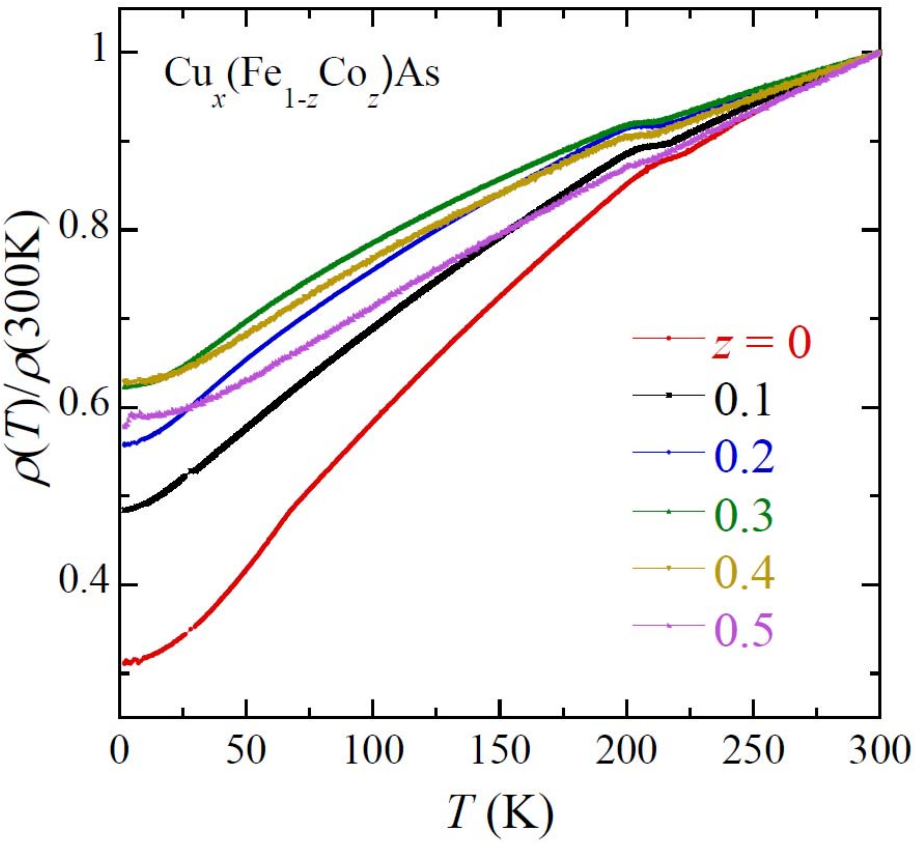
Cu$_x$(Fe$_{1-z}$Co$_z$)As
$\rho(T)/\rho(300K)$
1
0.8
0.6
0.4
0
50
100
150
200
250
300
T (K)
z = 0
0.1
0.2
0.3
0.4
0.5